BOREAL ENVIRONMENT RESEARCH 10: 525–541 ISSN 1239-6095
Helsinki 14 December 2005

A combined photochemistry/aerosol dynamics model: model development and a study of new particle formation

Alf Grini[1)2)], Hannele Korhonen[3)], Kari E. J. Lehtinen[4)], Ivar S. A. Isaksen[1)] and Markku Kulmala[2)]

[1)] *Department of Geosciences, University of Oslo, P.O. Box 1022 Blindern, N-0315 Oslo, Norway*
[2)] *Department of Physical Sciences, P.O. Box 64, FI-00014 University of Helsinki, Finland*
[3)] *Finnish Meteorological Institute, Research and Development, Erik Palmenin Aukio 1, P.O. Box 503, FI-00101 Helsinki, Finland*
[4)] *Finnish Meteorological Institute and University of Kuopio, Department of Applied Physics, P.O. Box 1627, FI-70211 Kuopio, Finland*

Grini, A., Korhonen, H., Lehtinen, K. E. J., Isaksen, I. S. A. & Kulmala, M. 2005: A combined photochemistry/aerosol dynamics model: model development and a study of new particle formation. *Boreal Env. Res.* 10: 525–541.

A new coupled photochemistry/aerosol model has been developed for studies of multicomponent aerosol dynamics. The photochemistry module, based on the reaction mechanisms of OSLO-CTM2 global model, has been extended with a simple oxidation scheme of volatile organic gases to produce condensable products. The aerosol module is a further development of UHMA (University of Helsinki Multicomponent Aerosol model) which incorporates all major aerosol dynamic processes with a special focus on new particle formation and growth. The new model explicitly incorporates production and loss terms from photochemistry into the calculation of condensation fluxes and nucleation rates, making the two models completely interactive. In this paper, we apply the new model to investigate the role of photochemistry and biogenic emissions in new aerosol formation and growth. Although using a simplified photochemistry scheme, the model allows for analysis of the evolution of chemical composition of an air mass simultaneously with the aerosol size distribution. The simulation results suggest a classification of air masses which goes beyond describing the air as "clean" or "polluted".

Introduction

Aerosol particles suspended in the Earth's atmosphere have significant effects on atmospheric chemistry, climate and human health. The particles alter the radiative balance of the Earth directly by absorbing and scattering incoming solar and outgoing thermal radiation (e.g. Charlson *et al.* 1991). Indirectly, particles affect the balance through clouds by modifying several cloud properties including albedo and lifetime (Twomey 1977, Albrecht 1989, Lohmann and Feichter 2005). The magnitude of especially the indirect effect remains, however, very uncertain (Intergovernmental Panel on Climate Change 2001). On the other hand, epidemiological studies have revealed a clear connection between elevated particulate load and hazardous public health effects, such as mortality, respiratory and cardiovascular hospital admissions, and the use

of asthma medication (Dockery *et al.* 1993, Atkinson *et al.* 1999, Künzli *et al.* 2000, Gordian and Choudhyry 2003).

It has now become evident that environmental effects of the atmospheric aerosol cannot be understood without understanding the processes that shape their number concentration, composition and size distribution (e.g. Ghan *et al.* 1998, Obot *et al.* 2002). Moreover, several of the most important aerosol dynamic processes, such as nucleation, condensation and cloud processing, involve interaction of the particles with gas-phase species. It is therefore vital that the evolution of aerosol particle populations is investigated concurrently with the chemistry of the gas-phase.

While experimental approaches provide invaluable data concerning the properties of ambient aerosol particles and gas-phase species, measurements are typically limited in spatial and temporal scales. Numerical model simulations, on the other hand, can extend from local to global scales and from fractions of a second to decades. They offer therefore a helpful tool to complement the ground and satellite based measurements. Furthermore, models provide access to information on aerosol dynamics and the interaction of the particles with the surrounding atmosphere that cannot be obtained with measurements alone.

Several models that simulate gas and particle phase processes simultaneously have been developed for regional and global scales (e.g. Lurmann *et al.* 1997, Bessagnet *et al.* 2004, Easter *et al.* 2004, Rodriguez and Dabdub 2004). While these kinds of large scale models offer a relatively realistic description of the aerosol mass (e.g. Takemura *et al.* 2000), they cannot include the complex processes needed for simulating aerosol number concentration and size realistically. On the other hand, zero-dimensional box models, which do not describe transport in space, can use all their computation time to describe the processes affecting the aerosol size and composition distribution in detail. Such models can thus provide insight into the microphysics and chemistry that govern the atmospheric effects of aerosols.

Earlier model studies of particle nucleation and growth have often focused on nucleation of sulfuric acid, or sulfuric acid and ammonia followed by further growth by condensation of sulfuric acid (Raes 1995, Pirjola *et al.* 1998, Katoshevski *et al.* 1999, Capaldo *et al.* 2000, Adams and Seinfeld 2002, 2003, Gaydos *et al.* 2005). Recent studies have shown that at remote sites the condensation of sulfuric acid can typically explain only about 10% of the observed growth rates (Birmili *et al.* 2003, Boy *et al.* 2005). On the other hand, modeling studies have suggested that at these sites low volatile organic vapours may contribute to the early stages of nanoparticle growth (Anttila and Kerminen 2003, Kulmala *et al.* 2004a). Furthermore, indirect composition measurements indicate that at forested sites most of the nucleation mode aerosol can actually be organic matter resulting from oxidation of biogenic vapors (O'Dowd *et al.* 2002).

In this study, we present a new combined box model of photochemistry and aerosol dynamics. The chemistry scheme is based on previously developed mechanism of OSLO-CTM2 (Berntsen and Isaksen 1997) and is extended in this study with a simplified organic scheme that mimics the essential condensation interaction of organic vapours with atmospheric particles. The size and chemistry resolved aerosol scheme bases on UHMA (University of Helsinki Multicomponent Aerosol model) (Korhonen *et al.* 2004) which is further developed in this study to a more flexible tool for different kinds of atmospheric studies. These two submodels are fully interactive and take explicitly into account the effect that various production and loss mechanisms of vapours have on condensation/evaporation as well as on nucleation.

We start by describing the photochemistry and aerosol modules of the new model. After that the new model is applied to study the effect of photochemistry on new particle formation and growth by gaseous compounds, which remains one of the least understood processes that alter the atmospheric aerosol distributions. Although particle formation is frequently observed in most parts of the world (Kulmala *et al.* 2004b), serious uncertainties surround the nucleation and growth mechanisms, not to mention the relative contribution of new particle formation to CCN concentrations and health effects of air pollution. The focus in our calculations is on the role of biogenic gas emissions, gaseous pollution and

competition between new particle growth and scavenging to pre-existing particles.

Photochemistry

The photochemistry scheme in the new model is based on the chemical mechanism of OSLO-CTM2 global chemical transport model (Berntsen and Isaksen 1997) which solves for the production and loss rates, and concentrations of the VOC/NO_x/HO_x system. The original scheme has been extended to include the sulfur cycle in the work of Berglen *et al*. (2004). The full chemistry mechanism has previously been applied to predict e.g. O_3/OH and other trace gases both in polluted and clean air masses (Sundet *et al*. 1997, Kraabøl *et al*. 2002, Endresen *et al*. 2003, Isaksen *et al*. 2005). In this study, the scheme has been extended to include a simplified organic mechanism in order to account for the atmospheric low volatile and semivolatile organic matter that condenses onto aerosol particles in the troposphere.

The following subsections describe the theoretical considerations and more detailed treatment of the chemistry scheme used in this study. In general, the modeled photolysis rates are calculated according to Wild *et al*. (2000) and depend on latitude and time of year. An assumed, climatological ozone column modifies the amount of arriving sunlight. The differential equations of the chemistry scheme are solved using the QSSA solver (Hesstvedt *et al*. 1978).

Oxidant chemistry

In the model, O_3 is produced through oxidation of methane and other hydrocarbons. If NO_x is present in the oxidation chain, O_3 is produced by HO_2/RO_2 radicals through

$$\begin{aligned} &NO + RO_2 \rightarrow NO_2 + RO \\ &NO_2 + h\nu \rightarrow NO + O. \\ &O_2 + O \rightarrow O_3 \end{aligned} \qquad (1)$$

The same processes are important in regulating concentrations of the OH radical which responds within seconds to chemical or physical (e.g. amount of sunlight) changes in the air mass. If NO_x is present, OH is constantly re-generated through

$$HO_2 + NO \rightarrow NO_2 + OH. \qquad (2)$$

However, in the absence of NO_x, OH is lost from the system through self-reactions between HO_2 molecules:

$$HO_2 + HO_2 \rightarrow H_2O_2 + O_2. \qquad (3)$$

One of the most important gas-phase compounds affecting the aerosol particle dynamics is H_2SO_4 whose concentration is regulated by OH and SO_2. The main sink for H_2SO_4 is condensation onto existing aerosol surfaces. Assuming steady state for H_2SO_4 gives

$$k[SO_2][OH] = CS \times [H_2SO_4] \qquad (4)$$

where k is a rate constant of the order of 10^{-12} cm^3 s^{-1}, and CS denotes condensation sink which is a measure of the vapour condensation rate onto aerosol population (in s^{-1}). Equation 4 shows that under a steady-state assumption and for given CS and SO_2 concentration, the gas-phase concentration of H_2SO_4 is directly proportional to the OH concentration.

Condensable organic vapors

Measurements indicate that organic matter can be responsible for close to or even more than 50% of the fine aerosol mass in the troposphere (Zappoli *et al*. 1999, O'Dowd *et al*. 2000). It is therefore vital to incorporate the transfer of organic mass from gas to particle phase into atmospheric models. Unfortunately, however, the majority of organic material found in the particulate phase remains unidentified.

Many of the organic compounds emitted directly from natural and anthropogenic sources are highly volatile and thus unable to contribute directly to aerosol mass. However, several studies have shown that atmospheric oxidation of the emitted compounds can yield vapours that possess volatilities much lower than their precursors (Pun *et al*. 2002). The oxidation paths that lead to low volatile products are often very complex (e.g.

Jenkin *et al*. 1997, 2000, 2002, Jenkin 2004). It seems clear, however, that such reaction chains always start either by O_3 adding to a double bond forming Criegee biradical (Atkinson and Carter 1984), or by NO_3 or OH subtracting a H atom from the parent hydrocarbon (Atkinson 1990). In general, a high molecular weight of the precursor compound (six or more carbon atoms) and polar groups (e.g. carboxylic COOH group) of the product compound tend to decrease the volatility (Chung and Seinfeld 2002, Seinfeld and Pankow 2003).

Given the complexity of oxidation mechanisms of hydrocarbons and the vast number of organic species found in the gas and aerosol phases, their detailed representation in a general photochemistry/aerosol model would be cumbersome, if not impossible. Because of this, the representation of organics is often simplified by lumping compounds with similar properties together or by assuming a two-product model

$$\mathrm{HC} + \mathrm{oxidants} \rightarrow p_1\mathrm{P}_1 + p_2\mathrm{P}_2 \qquad (5)$$

where p_1 and p_2 are molar stoichiometric coefficients, and P_1 and P_2 are the product compounds (Seinfeld and Pankow 2003).

The lumping of organic species can be done on the basis of several compound properties, such as volatility, molecular structure, water solubility, or origin. While the best suited lumping method depends to some extent on the purpose of the model, Bian and Bowman (2005) concluded that a combination of volatility and water interaction, or volatility alone as lumping criterion often produces the optimum results. In our model, we choose a highly simplified organic scheme in which we lump the compounds into three groups according to their saturation vapour pressure. We represent the fraction of volatile organic compounds which is able to react to form low volatile and semivolatile products by a single lumped gas denoted by $\mathrm{OC}_{\mathrm{hv}}$. This compound is assumed to remain totally in the gas phase. The two other organic model compounds, which are formed in oxidation reactions of $\mathrm{OC}_{\mathrm{hv}}$, represent the low and semivolatile vapours. These compounds are denoted by $\mathrm{OC}_{\mathrm{lv}}$ and $\mathrm{OC}_{\mathrm{sv}}$, respectively. Whereas the former resides mostly in the particle phase, the latter transfers reversibly between the gas and particle phases depending on the ambient conditions.

The model scheme assumes that the oxidation of $\mathrm{OC}_{\mathrm{hv}}$ proceeds via the following generalized reaction

$$\mathrm{OC}_{\mathrm{hv}} + \mathrm{OXI}_k \rightarrow Y_{k,\mathrm{lv}}\mathrm{OC}_{\mathrm{lv}} + Y_{k,\mathrm{sv}}\mathrm{OC}_{\mathrm{sv}} \qquad (6)$$

where OXI_k represents either hydroxyl radical (OH), nitrate radical (NO_3) or ozone (O_3), and corresponding values of Y_k represent the molar yields of the product compounds. The reactions of the organic high volatile compound $\mathrm{OC}_{\mathrm{hv}}$ with all these three oxidation agents are considered throughout the simulation. In practice, however, the reaction with NO_3 is important only at night because of the quick photolysis of NO_3 in daytime. Similarly, the OH reaction operates only in daytime whereas the O_3 reaction can operate both during night and day.

In theory, the values of Y_k are different for all components and oxidants. However, the actual atmospheric yields are difficult to quantify and we have therefore assumed equal yields for all oxidants (*see* Table 1). Rate coefficients for the reactions of $\mathrm{OC}_{\mathrm{hv}}$ are at 298 K (in $\mathrm{cm^3\ s^{-1}}$): 11650×10^{-18} for the O_3 reaction, 245×10^{-12} for the OH reaction, and 27×10^{-12} for the NO_3 reaction. These values were used for one hydrocarbon class by Chung and Seinfeld (2002). Using normal concentrations of oxidants, $\mathrm{OC}_{\mathrm{hv}}$ has lifetimes of minutes for the O_3 reaction and around one hour for the OH reaction. These are also the timescales by which $\mathrm{OC}_{\mathrm{hv}}$ will approach its new equilibrium concentration following a change in any oxidant concentrations.

It is important to realize that our mechanism for producing condensable organic vapors takes into account only the first step in a complex reaction chain. What happens in the reaction pathways in the following steps remains an open question. It has been suggested, for example, that the existence of NO_x in the airmass contributes to the formation of PAN-like components instead of low volatile organic acids (Jenkin *et al*. 2000). It is also unclear to what degree such a change in reaction mechanism would change the saturation vapor pressures of the low and semivolatile products.

Our three-component mechanism is very simplified as compared with many other more detailed schemes for secondary organic aerosol formation and photochemistry (e.g. Andersson-Skold and

Simpson 2001, Griffin *et al*. 2002). However, such sophisticated schemes are often evaluated only against chamber measurements which may not hold true for all ambient conditions. Furthermore, although several individual compounds which met in the atmosphere are inevitably borderline species in our schematic treatment, using lumped groups with distinct volatilities is likely to capture the general features that organic compounds have on aerosol dynamics. When using the organic scheme described here, one must however keep in mind its limitations. The scheme is most suitable for testing simple conceptions and hypothesis, as well as for sensitivity studies. In the future, elaboration of the organic mechanism is a logical next step in the development of the model.

Treatment of condensation in aerosol module

General description

The aerosol module is a further development of UHMA (University of Helsinki Multicomponent Aerosol model) (Korhonen *et al*. 2004) which is a size and composition resolved box model simulating the major aerosol physical processes in the atmosphere. The original model version described aerosol formation via emissions and homogeneous nucleation, growth by condensation of sulfuric acid and organic vapours, and particle loss via coagulation and dry deposition. In this study, we have coupled UHMA with thermodynamic equilibrium model ISORROPIA (Nenes *et al*. 1998) which has enabled the treatment of aerosol phase nitrate, ammonia and sea salt, the latter of which is not discussed in this paper. Furthermore, we have improved the numerical description of condensation and made the aerosol dynamic processes fully interactive with gas-phase chemistry. The improvements made to the aerosol scheme are described below. For further information on the aerosol model structure and subroutines, we refer the reader to the original model description in Korhonen *et al*. (2004). A kinetic nucleation formulation is used in this study, meaning that the nucleation rate is limited by the collision rate of sulphuric acid molecules through the reaction

$$J = 0.5KC^2 \quad (7)$$

where J is the nucleation rate, and K the collision rate of two gas-phase ammonium bisulphate molecules whose concentration is denoted with C.

Photochemical reactions affect aerosol dynamics through production and loss of vapors which can condense onto or evaporate from the aerosols, or nucleate to form new particles. In our model, we use time splitting and solve for nucleation before condensation/evaporation. Therefore, when coupling the equations for pho-

Table 1. Values used in the standard run.

Parameter	Physical meaning	Summer value	Spring value
Julian day	Day of year	182	91
RH_{max}	Max. diurnal relative humidity (03:00)	0.9	0.9
T_{min}	Min. diurnal temperature (03:00)	288 K	280 K
T_{max}	Max. diurnal temperature (15:00)	298 K	290 K
N_1	Number concentration, initial aerosol	8×10^8 m^{-3}	8×10^8 m^{-3}
σ_1	Standard deviation, initial aerosol	1.25	1.25
NMD_1	Number median diameter	4×10^{-8} m	4×10^{-8} m
N_2	Number concentration, initial aerosol	7×10^7 m^{-3}	7×10^7 m^{-3}
σ_2	Standard deviation, initial aerosol	1.25	1.25
NMD_2	Number median diameter	2×10^{-7} m	2×10^{-7} m
Y_{lv}	Yield of low volatile organic	0.1	0.1
Y_{sv}	Yield of semi volatile organic	0.9	0.9
E_{hv}	Emissions of organic volatile gas	5.0×10^9 cm^{-2} sec^{-1}	2.5×10^9 cm^{-2} sec^{-1}
$P^0_{sat,OCsv}$	Saturation vapor pressure OC_{sv}	10^{-7} Pa	10^{-7} Pa
SO_2	Mixing ratio of SO_2	0.5 ppb	0.5 ppb
NO_x	Mixing ratio of NO_x	40 ppt	40 ppt

tochemical production and loss, and the equation for condensation, we get the following equation which governs the gas phase concentrations

$$\frac{dC_{\infty,j}}{dt} = P_{\mathrm{chem},j} - \sum_{i=1}^{N} \frac{dc_{i,j}}{dt} - L_{\mathrm{chem},j} C_{\infty,j}. \quad (8)$$

Here $C_{\infty,j}$ is the ambient concentration of compound j, and $P_{\mathrm{chem},j}$ is its chemical production (m^{-3} s^{-1}) and $L_{\mathrm{chem},j}$ represents its chemical loss (s^{-1}). The second term on the right-hand side describes the interaction of the vapour with the aerosol particles. In this term $c_{i,j}$ represents the concentration of compound j in the model size section i, and N is the total number of size sections used in the model to represent the particle size distribution.

Onto any size section i of the model the flux of condensable compound j is given by the equation

$$\begin{aligned} \frac{dc_{i,j}}{dt} &= 2\pi \left(D_j + D_{\mathrm{p},i}\right)\left(d_{\mathrm{p},i} + d_j\right) \\ &\quad \times N_i \beta_i \left(C_{\infty,j} - C_{\mathrm{eq},i,j}\right) \\ &= k_{i,j}\left(C_{\infty,j} - C_{\mathrm{eq},i,j}\right) \end{aligned} \quad (9)$$

where $C_{\mathrm{eq},i,j}$ is the equilibrium concentration of j over the surface of a particle in section i (in m^{-3}). The diffusion coefficients and diameters of the vapor and the particle are denoted with D_j and $D_{\mathrm{p},i}$, and with d_j and $d_{\mathrm{p},i}$ respectively. N_i and β_i are the number concentration and transition regime correction factor for size section i. In this work, we used for β_i the formulation suggested by Fuchs and Sutugin (1971). Equation 9 is simplified denoting all terms dealing with gas phase diffusion $k_{i,j}$, which is now a loss rate (in s^{-1}). $(C_{\infty,j} - C_{\mathrm{eq},i,j})$ is a thermodynamic driving force.

In accordance with Eqs. 8 and 9, we can describe the mass balance of component j over a timestep Δt with

$$\begin{aligned} &C_{\infty,j}\left(t+\Delta t\right) + \sum_{i=1}^{N} c_{i,j}\left(t+\Delta t\right) \\ &= C_{\infty,j}\left(t\right) + \sum_{i=1}^{N} c_{i,j}\left(t\right) \\ &+ \Delta t\left[P_{\mathrm{chem},j} - L_{\mathrm{chem},j} C_{\infty,j}\left(t+\Delta t\right)\right] \end{aligned} \quad (10)$$

Equation 10 holds true for an infinitesimally short timestep, and provides an approximation of the concentration balance if the ambient vapour concentration $C_{\infty,j}$ cannot be considered constant over the timestep.

Numerical solver

Since the ambient vapour concentration $C_{\infty,j}$ and the condensation flux onto particles are strongly interdependent, Eqs. 8 and 9 need to be solved simultaneously. In the model, the chemical production and loss rates of semivolatile vapours are calculated in the photochemistry module, and they are then passed on to the aerosol module where the gas phase concentrations are calculated using a modified version of the Analytical Predictor of Condensation scheme (APC) (Jacobson 1997a).

We can obtain an expression for the concentration of compound j in size section i by integrating Eq. 9 over the timestep which yields

$$\begin{aligned} &c_{i,j}(t+\Delta t) = c_{i,j}(t) \\ &+ k_{i,j}\Delta t(C_{\infty,j}(t+\Delta t) - C_{\mathrm{eq},i,j}(t)). \end{aligned} \quad (11)$$

Inserting this into Eq. 10 and solving for the ambient vapour concentration yields (Jacobson 1997a)

$$\begin{aligned} &C_{\infty,j}\left(t+\Delta t\right) = \\ &\frac{C_{\infty,j}\left(t\right) + \sum_{i=1}^{N} k_{i,j}\Delta t C_{\mathrm{eq},i,j}\left(t\right) + \Delta t P_{\mathrm{chem},j}}{1 + \sum_{i=1}^{N} k_{i,j}\Delta t + \Delta t L_{\mathrm{chem},j}}. \end{aligned} \quad (12)$$

The terms in the numerator represent the vapour concentration in the previous time step, and the amounts of vapour that evaporate from the particle phase and is produced in chemical reactions, respectively. On the other hand, the two last terms in the denominator represent the amounts of vapour condensing onto the particles and lost in chemical reactions.

Equation 12 can be used to calculate the concentration of the compound j in all aerosol size sections. However, in case of evaporation, it is possible that the model predicts that a higher amount of the component is released to the gas phase than actually exists in the aerosol phase. When the mass flux is away from the particles, we check this for each size section i, starting from the smallest one since it is most likely to show evaporation and since it typically contains the smallest amount of component j. If too much mass evaporates, we use the following procedure:

1. Remove all the mass of component j from size section i and add it to the term $C_{\infty,j}(t)$ in Eq. 12.
2. For the size section i, set transfer coefficient of component j to zero.
3. Recalculate $C_{\infty,j}(t + \Delta t)$ from Eq. 12.
4. Treat section $i + 1$.

This procedure is repeated until either all mass is evaporated from all size sections, or until none of the sections lose more mass than is available in the particle phase.

Calculation of equilibrium vapor pressures

Inorganic compounds

The vapor pressure of sulfuric acid under atmospheric conditions is very low and is assumed to be zero in the model. Thus for sulfuric acid, Eq. 8 reduces to

$$\frac{dC_{\infty,j}}{dt} = P_{\text{chem},j} - \left(\sum_{i=1}^{N} k_{i,j} + L_{\text{chem},j} \right) C_{\infty,j} \quad (13)$$

which can be solved analytically as

$$C(t+\Delta t) = C(t)\exp\left[-\Delta t \left(\sum_{i=1}^{N} k_{i,j} + L_{\text{chem},j} \right) \right] + \frac{P}{\sum_{i=1}^{N} k_{i,j} + L_{\text{chem},j}} \times \left\{ 1 - \exp\left[-\Delta t \left(\sum_{i=1}^{N} k_{i,j} + L_{\text{chem},j} \right) \right] \right\} \quad (14)$$

Mass balance over the time step gives the condensation flux of sulfuric acid as:

$$J_{H_2SO_4} = \left[P_{\text{chem},j}\Delta t - C(t+\Delta t) + C(t) \right] \times \frac{\sum_{i=1}^{N} k_{i,j}}{\Delta t \left(L_{\text{chem},j} + \sum_{i=1}^{N} k_{i,j} \right)} \quad (15)$$

Condensation of NH_3 is closely coupled with condensation of H_2SO_4 and HNO_3 since they all change the acidity of the aerosols. For NH_3 and HNO_3, the equilibrium vapour concentrations are determined for each particle size section separately based on the thermodynamic equilibrium model ISORROPIA (Nenes *et al*. 1998). To avoid oscillations in the solutions when the acidity of the particles fluctuates between levels slightly smaller and slightly larger than the equilibrium, we modify the condensation fluxes of NH_3 and HNO_3 according to the method of Pilinis *et al*. (2000). This method limits the maximum flux of H^+ by

$$\left| J^{\max}_{H^+,i} \right| = A_i C_{H^+,i} \quad (16)$$

where $J_{H^+,i}$ is the flux of H^+ (s^{-1} m^{-3}), A_i is the allowed rate of change of aerosol acidity (in this study 0.01 s^{-1}), and $C_{H^+,i}$ is the concentration of H^+ in the size section (m^{-3}). The flux of H^+ is given by

$$J_{H^+} = J_{HNO_3} + 2J_{H_2SO_4} - J_{NH_3}. \quad (17)$$

Here we assume full dissociation of the dissolved inorganic compounds. In case the flux of H^+ exceeds the maximum value given by Eq. 16, the equilibrium vapor pressures of NH_3 and HNO_3 are adjusted in order to meet the limit (*see* Pilinis *et al*. (2000) for more details).

Organic compounds

The general formulation of the model allows to freely choose the saturation vapor pressures of the lumped low volatile and semivolatile organic groups. In this study, we used the following values: For OC_{lv}, the equilibrium vapor pressure is assumed to be zero, and thus the fluxes and concentrations can be calculated similarly to sulfuric acid (*see* Eqs. 14 and 15). Although technically this compound is treated as non-volatile, we still choose to call it low volatile since in nature no vapours show exact zero volatility.

For OC_{sv}, we assumed that it is absorbed in the particulate organic phase above which its equilibrium vapor pressure was set to a value that is dependent on the temperature according to Clausius-Clapeyron equation with a value of $\Delta H_{evap}/R$ = 6000 K. The equilibrium vapor pressure of OC_{sv} is also adjusted for curvature

effects, increasing equilibrium vapor pressure for the smallest particles. Only in cases with high photochemical production of OC_{sv}, its vapor pressure can increase beyond the value needed to grow the smallest nucleation mode particles. In the case of lower production, the vapor pressure will approach the equilibrium concentration of the larger aerosols according to Eq. 12. The saturation vapour pressures used for OC_{sv} are presented in Tables 1 and 2. Despite the relatively low saturation pressures, we call the compound semivolatile to reflect that it will not condense onto all aerosol size classes but still can partition between gas and aerosol phase.

Our assumptions mean that we largely simplify gas/aerosol thermodynamics. We do not, for example, consider that the organic component can partition into the aquous phase of the aerosol, neither do we use the composition of the organic aerosol phase to calculate the equilibrium vapor pressure of the condensable organics. Such thermodynamic frameworks do exist in the literature (for example Pun *et al*. (2002) and references therein) but are poorly applicable to our simplified modelling frame. The reason is that all the semivolatile components are lumped into only one species, and there is therefore relatively little room for changing mole fraction of the different condensable organic compounds in the aerosol.

Effect of photochemistry on new particle formation

Motivation

The combined model will in later work be applied to analyse measurement data of new particle formation from several field sites. For this paper, such comparisons with observations are beyond the scope; however, we wish to make some general theoretical remarks concerning the effect of photochemistry on new particle formation and growth.

In the Scandinavian boreal forest region, new particle formation events are frequently observed especially in the spring and autumn (Vehkamäki *et al*. 2004, Dal Maso *et al*. 2005). However in summer, when the solar radiation and thus the photo-oxidation rates reach their yearly maximum values, particle formation is detected on much fewer days. One of the explanations for this spring maximum has been the arrival direction of the air masses to the region: in spring and autumn the prevailing air masses are from the Arctic and polar areas and contain relatively low pre-existing aerosol concentrations, whereas in summer the warm air from the southerly sector sometimes carries a high pre-existing aerosol load that can suppress new particle formation.

In this study, we explore another possible explanation to the formation event minimum in summer. We test the hypothesis that the role of enhanced biogenic emissions in summer could inhibit the growth of nucleated particles to detectable sizes. The two-fold effect of the enhanced formation rate of the organic oxidation products can be summarized as follows:

1. Oxidation of highly volatile organic compounds yields products which grow the nucleated clusters to larger sizes. These products are represented by OC_{lv} in our study.
2. At the same time, oxidation of highly volatile compounds is a source of low and semivolatile products which grow the background aerosol and thus increase the coagulation sink for the nucleated particles. These products are represented by OC_{sv} in our study.

Table 2. Sensitivity studies performed with the model.

Run number	Run name	Variation	Explanation
2	HIGHLV	$Y_{lv} = 0.20$; $Y_{sv} = 0.80$	Higher yield of low volatile organic
3	LOWLV	$Y_{lv} = 0.01$; $Y_{sv} = 0.99$	Lower yield of low volatile organic
4	VOL_SV	$10.0 \times P^0_{sat,OCsv}$	Higher pressure of semi volatile organic
5	LOWVOL_SV	$0.1 \times P^0_{sat,OCsv}$	Lower pressure of semi volatile organic
6	NOX	$NO_x = 400$ ppt	Increased NO_x

Essentially, this means that the newly formed nanoclusters cannot grow by condensation unless the background aerosol also grows and thus increases the coagulation sink for the clusters. In this study, we investigate this competition mechanism with a set of sensitivity simulations. We also investigate the importance of knowing the composition of the gas phase when analysing nucleation events. We show that increasing the concentration of NO_x can, through changing OH concentrations, change the aerosol dynamics. Some earlier aerosol dynamics studies have fixed OH to follow daily cycles decoupled from the rest of the gas phase chemistry (e.g. Anttila *et al*. 2004, Gaydos *et al*. 2005).

The simulations presented below are by no means conclusive. Still, they demonstrate the complex role of photochemistry on new particle formation mechanisms and highlight that aerosol dynamics can seldom be simulated in isolation from the gas-phase reactions.

Simulation conditions

The simulations were conducted for a 24-hour period starting at midnight. For simplicity, we assumed the temperature to follow a sinusoidal curve with a maximum at 15:00 and a minimum at 03:00. We assumed also that the specific humidity (kg (H_2O) kg^{-1} (air)) was constant during the simulation, and thus that the relative humidity reached its maximum at the same time as the temperature reached its minimum value. Although somewhat simplified, these assumptions imitate general features of the diurnal variations in temperature and relative humidity at the simulated region. The simulations were made for a site lying on latitude 60°. On the simulated spring and summer days, the photolysis rates were adjusted according to the simulated solar radiation, which followed the normal diurnal pattern at the corresponding latitude.

The background aerosol distribution (assumed bimodal) and the vapour concentrations and emission rates used as input in the standard (base case) simulations are presented in Table 1. In order to isolate the effect of organic emissions and photochemistry on particle concentrations, the simulations for both spring and summer conditions were made with the same initial particle size distribution.

The emissions of reactive biogenic volatile organic vapor were chosen to be 5×10^9 cm^{-2} s^{-1} for summer and 2.5×10^9 cm^{-2} s^{-1} for spring. These values translate to 0.3 and 0.15 g(C) m^{-2} yr^{-1} assuming 10 C atoms per molecule emitted. Guenther *et al*. (1995) propose that isoprene emissions from boreal forests peak in July. Assuming that our volatile organic gas behaves like isoprene it seemed logical to include a higher summer than spring emission, although the factor of two is somewhat arbitrarily chosen. Guenther *et al*. (1995) propose around 1 g(C) m^{-2} yr^{-1} reactive BVOC for forested summer conditions, and assuming 30% of this will react to low and semi volatile products might be too much. However, our simulations give OC_{lv} and OC_{sv} concentrations of some ppts which Kulmala *et al*. (2004a) indicated are needed to correspond to observed growth rates.

With the chosen emissions, the lifetime of OC_{hv} is of the order of five minutes with respect to O_3 and one hour with respect to OH. With our box extending to 1000 m (approximately the height of the boundary layer), the steady state concentration of OC_{hv} is approximately of the order of 0.1–1 ppt. This is much lower than concentrations of high volatile compounds, such as monoterpene, which can be of the order of ppb. With this in mind, it is important to note that all of OC_{hv} is reactive whereas not necessarily all monoterpenes are reactive; in other words, OC_{hv} represents only that fraction of atmospheric volatile organic compounds which can produce condensable compounds.

The sensitivity runs for the interaction of new particle formation and growth to the gas-phase chemistry are summarized in Table 2. The runs investigate how the percentual yield of organics with different volatility, the saturation vapour pressure of the semivolatile compounds and the increase of NO_x influence the particle formation.

As compared with the base case, runs 2 and 3 do the opposite things. In run 2, the increase in the yield of low volatile compound OC_{lv} could potentially increase the growth of newly formed particles. However, this run will also increase the size of the background particles since more of the oxidation product goes to the aerosol phase.

On the other hand, run 3 decreases the yield of OC_{lv}. Consequently, this decreases the amount of oxidation product which can condense on the smallest aerosols.

The second pair of sensitivity simulations, i.e. runs 4 and 5, investigate the sensitivity of the system to the saturation vapour pressure of the semivolatile compound OC_{sv}. Higher saturation pressure (run 4) increases the smallest size of particles which can grow by condensation of OC_{sv}, and thus nucleated clusters need to be able to grow to larger sizes with the low volatile compound OC_{lv} and H_2SO_4 as the only condensing species. On the other hand, the background aerosols would also grow more slowly. Conversely, in run 5 the lower saturation vapour pressure decreases the critical size of particles above which the OC_{sv} can condense on them. On the other hand, also the background aerosols grow more quickly in this run.

As compared with the rest of the simulations, run 6 uses a tenfold concentration of NO_x, i.e. 400 ppt. According to Wayne (2000), this value is still at the upper limit of clean air classification. The increased NO_x concentration will affect the oxidant concentrations and the daily cycle of oxidation rates change.

Results and discussion

General observations

As shown in Table 1, the spring simulations differ from the summer ones by lower emissions of biogenic volatile organic vapor (OC_{hv}), less sunlight and lower temperatures. The number concentrations for different sized particles from the runs for both seasons are presented in Fig. 1. The zigzag alterations in the concentrations are caused by the description of the particle size distribution in our model. We use the moving center method (Jacobson 1997b) which is in most respects advantageous for combined condensation and nucleation simulations but produce alterations in concentrations plotted as in Fig. 1 (Korhonen *et al*. 2004).

In many respects the results for spring and summer are very similar. The aerosol number concentration starts to increase immediately after sunrise, which takes place approximately two hours later in spring (Fig. 1a and e). This is connected to the onset of H_2SO_4 formation which in turn is controlled by photochemical production of OH radical (Figs. 2 and 3). The higher production of OH in summer, due to more UV radiation than in spring, is also responsible for the clearly higher formation rate of new particles.

Panels b–d and f–h in Fig. 1 show that the formed particles grow much faster under chosen summer than spring conditions, respectively. The reasons for this is mainly the higher emission rate of volatile organics, represented in our model with OC_{hv}, which yields also higher concentrations of low and semivolatile compounds (Figs. 2 and 3). OC_{lv} is mainly responsible for the growth of the formed particles; in our simulations it is capable of condensing onto all-sized particles and thus accelerates the growth of the nanoclusters. In addition, the semivolatile compound OC_{sv}, which contributes to the growth once the particles have reached a sufficient size, is also produced in greater amounts in summer. The concentration of sulfuric acid is much lower than that of organics and its contribution to the growth of the formed particles is relatively small. It is interesting to note, however, that despite the higher summer time nucleation rate, i.e. higher loss rate of H_2SO_4 due to nucleation, its predicted ambient concentration remains slightly higher in summer than in spring.

In contrast to what is observed, the simulations predict consistently a higher concentration of nucleation mode particles at 10 nm and beyond in summer. This is true although also the condensation sink, which is a measure of the potential depletion rate of condensing vapor molecules to the whole aerosol population, is slightly higher in summer than in spring (Fig. 4). In principle, a high CS value implies that more condensable vapor is lost to the background particles and less of it is available for nanocluster growth, and that more of these clusters are scavenged by coagulation. Since the survival rate of nucleation mode particles is a strong function of size, the newly formed particles need to grow fast in order to reach detectable sizes when the CS is high. Because of the fast growth of nucleation mode particles in summer, even the higher CS cannot eliminate all the formed particles. Furthermore,

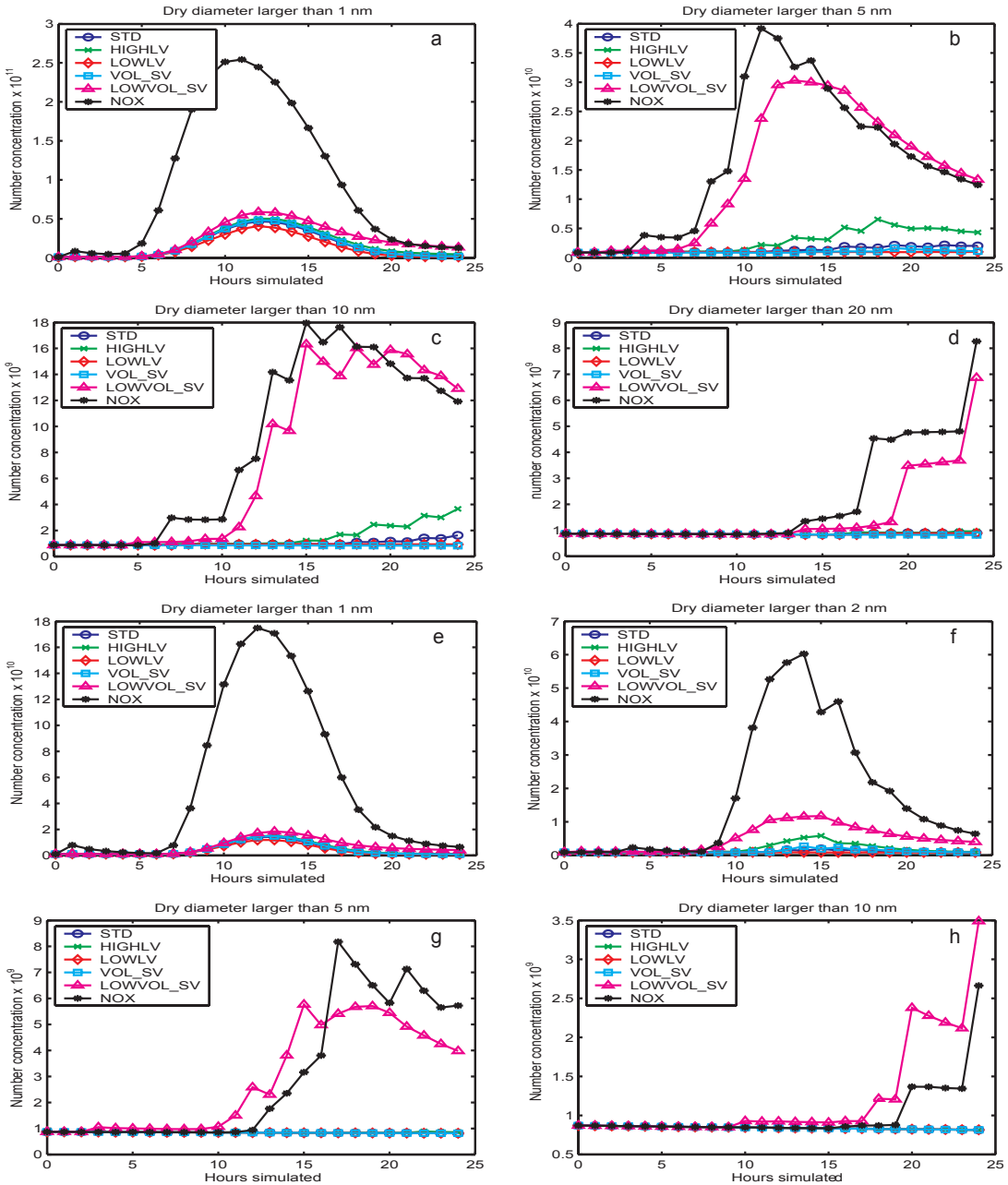

Fig. 1. Aerosol number concentrations (# m^{-3}) simulated during the day which are larger than the sizes indicated on the top of the figure form summer (**a**–**d**) and spring (**e**–**h**). The legends of the figure are explained in Table 2. Note that spring and summer figures do not show the same sizes, since in summer, condensation is more rapid, and aerosols grow more quickly to larger sizes.

despite the high difference in organic emissions and radiation, the difference between the summer and spring sinks is small in the morning hours, which is the relevant time regarding nanoparticle growth. Starting with identical particle distributions, the CS values at 10:00 (excluding the NOX run) are 1.4–1.5 s^{-1} for summer conditions and 1.25–1.3 s^{-1} for spring conditions. It is therefore unlikely that higher biogenic vapor emissions and enhanced photochemical activ-

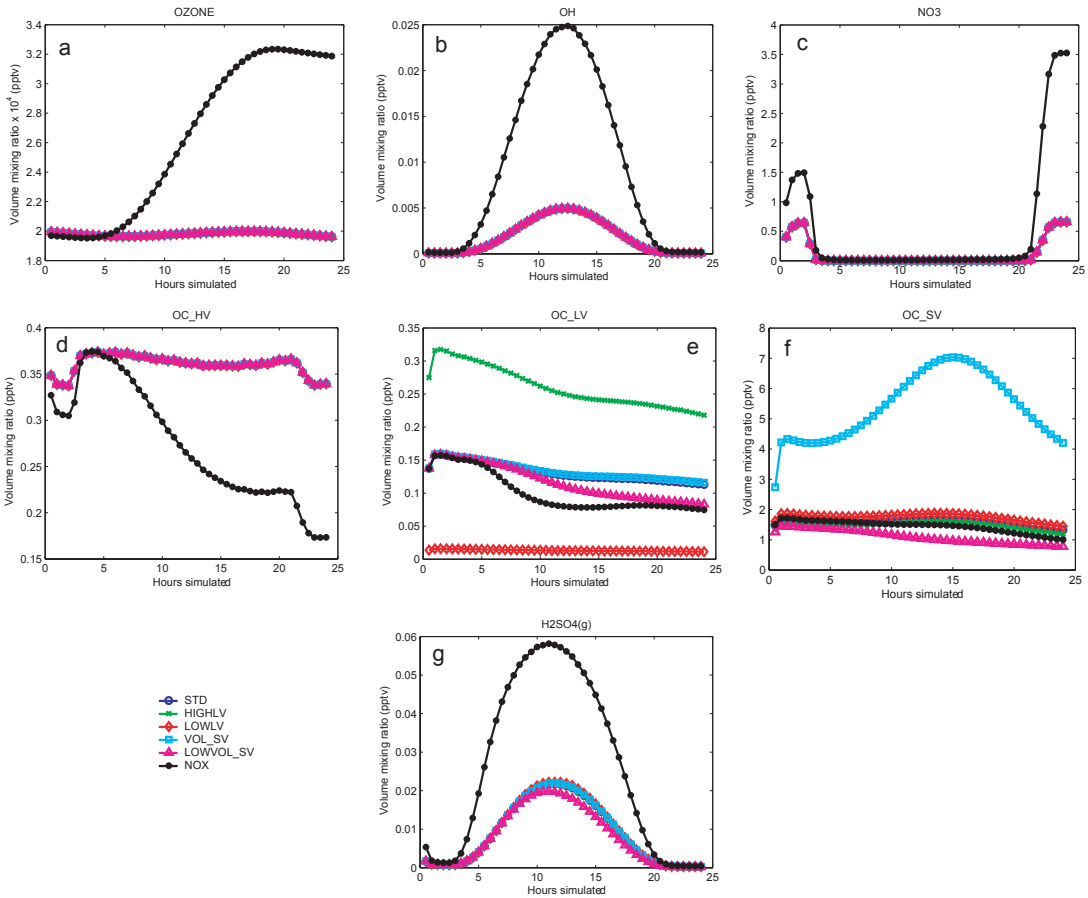

Fig. 2. Summer conditions: concentrations of gases important for controlling aerosol growth. The legends are explained in Table 2.

ity in summer could alone explain the observed minimum in new particle formation events.

Sensitivity analysis

Of the sensitivity runs, NOX and LOWVOL_SV give clearly the most new particles at large sizes (Fig. 1). The reasons for efficient particle production in these two cases are, however, different: In the LOWVOL_SV run, the low vapour pressure of OC_{SV} makes it possible for this gas to condense on the smallest aerosols. On the other hand, the high concentrations of new particles in the NOX run stem from the higher formation rate of H_2SO_4. Not only does this yield higher nucleation rates but also significantly faster growth of nanocluster by condensation of H_2SO_4.

We find that two runs in which most new particles survive to large sizes (i.e. NOX and LOWVOL_SV) also show the largest CS values. This result seems to contradict the original possibility that high CS would deplete nucleated clusters more rapidly than they are able to grow to larger sizes. In the NOX run, there is a very large increase in CS from 10:00 to 15:00, i.e. the same period when the total number concentration increases due to nucleation. The significant contribution of new particles to the sink can be seen after 15:00 when the CS actually decreases because of end of nucleation and because of coagulation scavenging of the existing nucleation mode particles. This is consistent with the results of Korhonen *et al.* (2005) who found that the nucleation event itself could contribute largely (up to 80%) to the change in the observed condensation sink during a

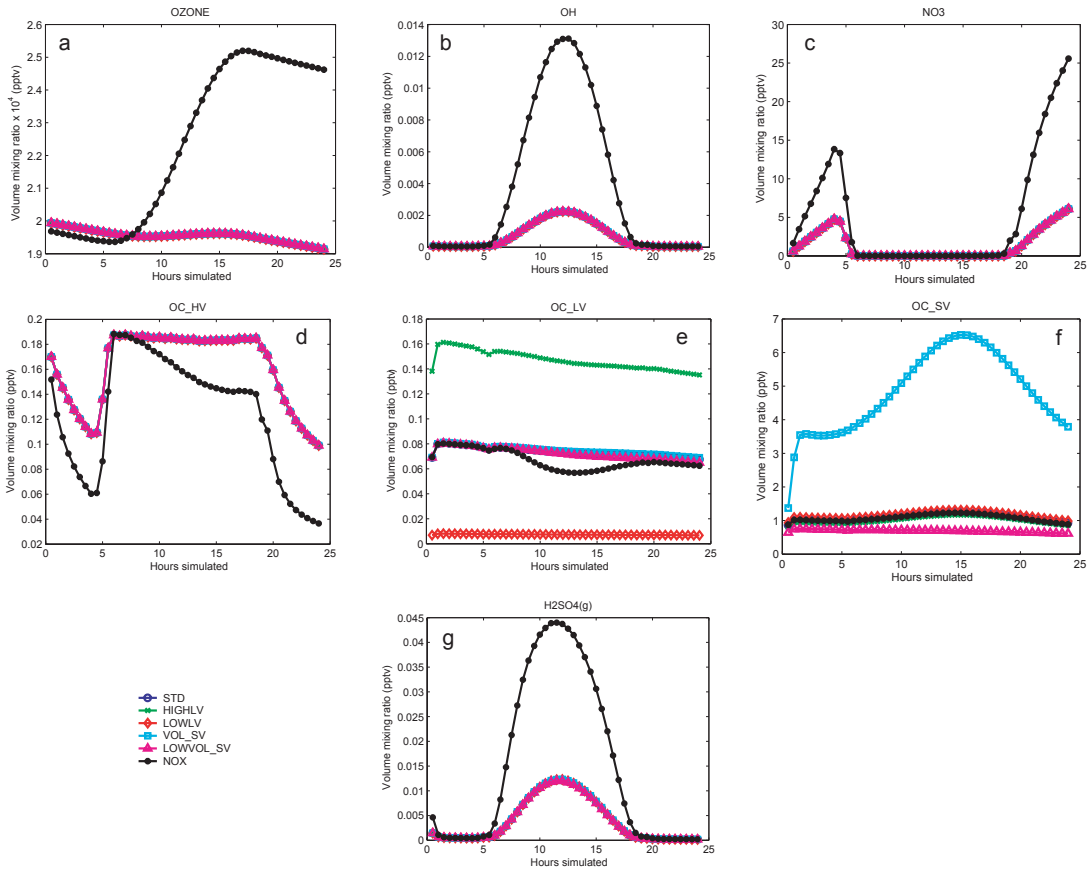

Fig. 3. Spring conditions: concentrations of gases important for controlling aerosol growth. The legends are explained in Table 2.

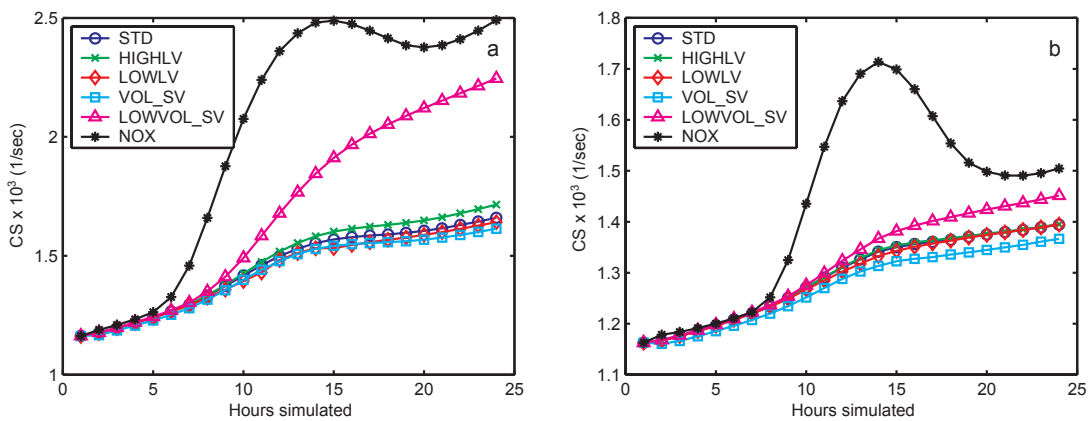

Fig. 4. Condensation sink (sec^{-1}) for OC_{LV} during the simulation for summer (**a**) and spring (**b**). The legends are explained in Table 2.

nucleation event. In the NOX run, the CS mainly increases because the larger OH concentrations give high H_2SO_4 concentrations which produce many clusters. In the LOWVOL_CS run, there are fewer clusters produced, but rapid growth transfers them efficiently to larger sizes.

The general features between the sensitivity runs in the concentrations of the gas-phase species are the same for spring and summer conditions (Figs. 2 and 3). It is noteworthy that the concentrations of oxidants OH, O_3 and NO_3 are identical in all summer simulations except the NOX simulation. In this simulation, additional O_3 is produced through Eq. 1, and OH is maintained through Eq. 2. At night, NO_x compounds are in the absence of sunlight transferred to NO_3.

In the NOX run, OC_{hv} is depleted more rapidly than in other runs due to higher oxidant concentrations. The concentrations of the oxidation products, OC_{lv} and OC_{sv}, are more complicated to interpret. The concentration of OC_{lv} is the highest in run HIGHLV, and the lowest in run LOWLV, reflecting its production rate. The small differences between the other runs are due to development of the condensation sink induced by the aerosol particles.

It is interesting to note that the NOX run has the second lowest concentrations of OC_{lv}. This result has to be interpreted in terms of production rates, loss rates and chemical lifetimes. In our model, all OC_{hv} reacts to form condensable species, so at steady state, the sum of the production rates of OC_{lv} and OC_{sv} equals emission rates of OC_{hv}. If the response time of OC_{lv} were long, increasing oxidants would increase production rates of condensable vapours until steady state were reached again. As this is not the case in our model, (the lifetime of OC_{hv} is minutes with respect to O_3 and about one hour with respect to OH), increasing oxidants does not increase production rates of condensable vapours. However, since CS, and thus the loss of OC_{lv} is large in the NOX run, OC_{lv} is efficiently depleted. This argument becomes clear considering the concentration of H_2SO_4. The concentration of SO_2 is not significantly depleted from the increased OH in the NOX run because the lifetime of SO_2 with respect to OH is longer. This allows production rates of H_2SO_4 to increase, and even though the large CS depletes H_2SO_4 in a similar way as it depletes OC_{lv} (Eq. 4), the concentrations of H_2SO_4 are large in the NOX run.

The concentration of OC_{sv} is the highest in the VOL_SV run and the lowest in the LOWVOL_SV run, reflecting its saturation vapor pressure. The high peak in the VOL_SV run at around 15:00 is due to the maximum of saturation vapor pressure which is dependent on temperature through the Clausius-Clapeyron equation. The NOX run gives the second lowest concentration also for OC_{sv}. The reasons for the low OC_{sv} are similar to the reasons for the low OC_{lv} except that the part of the CS which is due to the very smallest particles is not accessible by OC_{sv}.

It is also interesting to note that the H_2SO_4 (g) concentration peaks around 10:00 in the NOX run, whereas OH peaks two hours later at around noon. This difference arises from the development of the condensation sink which increases rapidly in the morning hours due to condensation and to a lesser extent due to nucleation. This increase makes the sink for H_2SO_4 (g) larger at 12:00 than at 10:00.

Uncertainties

The presented model suffers from several uncertainty factors. Firstly, when using values for reaction rates for organic vapors with the major oxidants, we were forced to pick values as input data to the model. In nature, these values can vary by orders of magnitude, so it is difficult to know which ones to use. In addition, since we do not know exactly which gases constitute OC_{hv} it is hard to estimate the actual emission rates.

Also, since we only simulate photochemistry and aerosol microphysics, we do not take into account other processes which are important for aerosol formation in the boundary layer. Naturally, one such process is boundary layer physics. Korhonen *et al.* (2005) found that the breakup of the nocturnal boundary layer may play an important role in the dynamics of morning nucleation events. Interestingly, this is often at the same time as the OH concentrations rise. Our current model does not, however, allow us to separate the two effects.

Conclusions and summary

We introduce a box model where a well-established photochemical scheme from OSLO-CTM2 (Berntsen and Isaksen 1997) is combined with an aerosol dynamics model UHMA (Korhonen *et al.* 2004). The chemistry module is further

developed with a simplified organic scheme. This scheme lumps the organic vapors encountered in the atmosphere into three groups according to their saturation vapor pressures, which control the condensation of the vapors onto aerosol particles. The aerosol module is extended to treat nitrate and sea salt with the thermodynamic equilibrium model ISORROPIA (Nenes *et al*. 1998). We also introduce a simple mathematical concept which couples condensation/evaporation equations of the aerosol dynamics directly to the photochemistry solver. The photochemistry and aerosol dynamic modules are fully interactive and the combined model can be used to study how production, loss and concentrations of photo oxidants evolve simultaneously with the aerosol size distribution. The model calculates the effect of gas emissions and photochemistry on the size and composition distribution of aerosols, and it contains an explicit feedback mechanism to the concentration of gaseous species.

In our example simulations, we discuss evolution of a boreal forest aerosol distribution in clean air masses. We use numerical simulations to study how photochemical processes together with biogenic emissions of organic gases affect new particle formation, and especially if they can provide an explanation why nucleation and growth events are more frequently observed in spring than in summer. The simulations indicate that, given that the initial airmasses have the same pre-existing aerosol population, the chosen summer conditions tend to produce more aerosols in contrast to observations. This is due to the growth rate of formed particles which is high enough to save a significant fraction of them from scavenging to the background particles, despite the higher coagulation sink than under spring conditions.

Interpreting the concentrations of gases together with the aerosol size distribution allows also insight into other complex and intercompeting processes. We find out for example that the cleanest airmasses are not necessarily the most favourable for particle production. More specifically, when NO_x is included in the airmass under summer conditions, the concentrations of low volatile organics, which result from oxidation of biogenic emissions and according to current knowledge are crucial in early stages of nanoparticle growth in boreal forest conditions (Anttila and Kerminen 2003, Kulmala *et al*. 2004a), are low. As an isolated observation, this would mean that small aerosols would grow more slowly and be lost by coagulation before they reach detectable sizes. However, in our simulations, the high NO_x concentration yields also high OH concentration which in turn converts more SO_2 to sulfuric acid. The very low volatile H_2SO_4 grows the particles and thus gives rise to high condensation sink which depletes much of the low volatile organic matter.

As shown in this study, understanding the chemistry of OH and other oxidants is vital for understanding the evolution of the aerosol size distribution. It is therefore an advantage for box model studies to be able to change the gas phase components which are the ones that can really be changed by advection and emissions (e.g. SO_2, NO_x, VOC). OH is very shortlived and will respond within seconds to the ambient conditions. Letting OH adjust to the airmass composition ensures consistency between the aerosol dynamics calculations and the microphysics calculations.

Our results encourage chemical analysis of airmasses which goes beyond classifying the airmass simply as "clean" or "polluted". A possible explanation for the observed peak of particle formation events in spring is that arctic airmasses bring clean air with low pre-existing aerosol mass. We propose that in order to explore this explanation, both chemical characteristics (gas phase concentrations) and physical characteristics (pre-existing aerosols) have to be known. Clean, polar air would typically contain low NO_x concentrations. This in turn is likely to restrict the concentration of OH and thus H_2SO_4, which is assumed to play a critical role in new particle formation.

Acknowledgements: The authors acknowledge support from the Nordic Center of Excellence (BACCI). AG acknowledges also support from the Norwegian research council grant 139810/720 (CHEMCLIM).

References

Adams P.J. & Seinfeld J.H. 2002. Predicting global aerosol size distributions in general circulation models. *J. Geophys. Res.* 107(D19), 4370, doi:10.1029/2001JD001010.

Adams P.J. & Seinfeld J.H. 2003. Disproportionate impact of particulate emissions on global cloud condensation nuclei concentrations. *Geophys. Res. Lett.* 30: 1239, doi:10.1029/2002GL016303.

Albrecht B. 1989. Aerosols, cloud microphysics, and fractional cloudiness. *Science* 245: 1227–1230.

Andersson-Skold Y. & Simpson D. 2001. Secondary organic aerosol formation in northern Europe: A model study. *J. Geophys. Res.* 106: 7357–7374.

Anttila T. & Kerminen V.-M. 2003. Condensational growth of atmospheric nuclei by organic vapors. *J. Aerosol Sci.* 34: 41–61.

Anttila T., Kerminen V.-M., Kulmala M., Laaksonen A. & O'Dowd C. 2004. Modelling the formation of organic particles in the atmosphere. *Atmos. Chem. Phys.* 4: 1071–1083.

Atkinson R. 1990. Gas-phase tropospheric chemistry of organic compounds: A review. *Atmos. Environ.* 24A: 1–41.

Atkinson R. & Carter W. 1984. Kinetics and mechanisms of the gas-phase reactions of ozone with organic compounds under atmopheric conditions. *Chem. Rev.* 84: 437–470.

Atkinson R., Bremner S., Anderson H., Strachan D., Bland J. & Ponce de Leon A. 1999. Short-term associations between emergency hospital admissions for respiratory and cardiovascular disease and outdoor air pollution in London. *Arch. Environ. Health.* 54: 398–411.

Berglen T., Berntsen T., Isaksen I. & Sundet J. 2004. A global model of the coupled sulfur/oxidant chemistry in the troposphere: The sulfur cycle. *J. Geophys. Res.* 109, doi:10.1029/2003JD003948.

Berntsen T. & Isaksen I. 1997. A global 3-D chemical transport model for the troposphere, 1, model description and CO and ozone results. *J. Geophys. Res.* 102: 21239–21280.

Bessagnet B., Hodzig A., Vautard R., Beekman M., Cheinet S., Honor C., Liousse C. & Rouil L. 2004. Aerosol modeling with CHIMERE: Preliminary evaluation at the continental scale. *Atmos. Environ.* 38: 2803–2817.

Bian F. & Bowman F. 2005. A lumping model for composition- and temperature dependent partitioning of secondary organic aerosols. *Atmos. Environ.* 39: 1263–1274.

Birmili W., Berresheim H., Plass-Dalmer C., Elste T., Gilge S., Wiedensholer A. & Uhrner U. 2003. The Hohenpeissenberg aerosol formation experiment (hafex): a long term study including size-resolved aerosol, H_2SO_4, OH, and monoterpene measurements. *Atmos. Chem. Phys.* 3: 361–376.

Boy M., Kulmala M., Ruuskanen T.M., Pihlatie M., Reissell A., Aalto P.P., Keronen P., Dal Maso M., Hellen H., Hakola H., Jansson R., Hanke M. & Arnold F. 2005. Sulphuric acid closure and contribution to nucleation mode particle growth. *Atmos. Chem. Phys.* 5: 863–878.

Capaldo K., Pilinis C. & Pandis S. 2000. A computationally efficient hybrid approach for dynamic gas/aerosol transfer in air quality models. *Atmos. Environ.* 34: 3617–3627.

Charlson R., Lagner J., Rodhe H., Leovy C. & Warren S. 1991. Perturbation of the northern-hemisphere radiative balance by backscattering from anthropogenic sulfate aerosols. *Tellus* 43: 152–163.

Chung S. & Seinfeld J. 2002. Global distribution and climate forcing of carbonaceous aerosols. *J. Geophys. Res.* 107, doi:10.1029/2001JD001397.

Dal Maso, M., Kulmala, M., Riipinen, I., Wagner, R., Hussein, T., Aalto, P. P. & Lehtinen, K. E. J. 2005: Formation and growth of fresh atmospheric aerosols: eight years of aerosol size distribution data from SMEAR II, Hyytiälä, Finland. *Boreal Env. Res.* 10: 323–336.

Dockery D., Pope C., Xu X., Sprengler J., Ware J., Fay M., Ferris B. & Speizer F. 1993. An association between air pollution and mortality in six U.S. cities. *N. Engl. J. Med.* 329: 1753–1759.

Easter R.C., Ghan S.J., Zhang Y., Saylor R.D., Chapman E.G., Laulainen N.S., Abdul-Razzak H., Leung L.R., Bian X. & Zaveri R.A. 2004. MIRAGE: Model description and evaluation of aerosols and trace gases. *J. Geophys. Res.* 109, doi:10.1029/2004JD004571.

Endresen Ø., Søgård E., Sundet J., Dalsøren S., Isaksen I., Berglen T. & Gravir G. 2003. Emission from international sea transportation and environmental impact. *J. Geophys. Res.* 108, doi:10.1029/2002JD00289.

Fuchs N. & Sutugin A. 1971. Highly dispersed aerosol. In: Hidy G.M. & Brock J.R. (eds.), *Topics in current aerosol research*, Pergamon, New York, pp. 1–60.

Gaydos T., Steiner C. & Pandis S. 2005: Modeling of in situ ultrafine atmospheric particle formation in the eastern United States. *J. Geophys. Res.* 110, D07S12, doi:10.1029/2004JD004683.

Ghan S., Guzman G. & Abdul-Razzak H. 1998. Competition between sea salt and sulfate particles as cloud condensation nuclei. *J. Atmos. Sci.* 55: 3340–3347.

Gordian M. & Choudhury A. 2003. PM_{10} and asthma medication in school children. *Arch. Environ. Health.* 58: 42–47.

Griffin R.J., Dabdub D. & Seinfeld J.H. 2002. Secondary organic aerosol 1. Atmospheric chemical mechanism for production of molecular consitituents. *J. Geophys. Res.* 107(D17), 4332, doi:10.1029/2001JD00541.

Guenther A., Hewitt C.N., Erickson D., Fall R., Geron C., Graedel T., Harley P., Klinger L., Lerdau M., McKay W.A., Pierce T., Scholes B., Steinbrecher R., Tallamraju R., Taylor J. & Zimmerman P. 1995. A global model of natural volatile organic compound emissions. *J. Geophys. Res.* 100: 8873–8892.

Hesstvedt E., Hov Ø. & Isaksen I. 1978. Quasi steady-state approximation in air pollution modeling: Comparison of two numerical schemes for oxidant prediction. *Intl. J. Chem. Kin.* X: 971–994.

Intergovernmental Panel on Climate Change (IPCC) 2001. *Climate change 2001: The scientific basis*. Cambridge University Press.

Isaksen I., Zerefos C., Kourtidis K., Meleti C., Dalsøren S., Sundet J., Grini A. & Balis D. 2005. Tropospheric ozone changes at unpolluted and semi-polluted regions induced by stratospheric ozone changes. *J. Geophys. Res.* 110, D02302, doi:10.1029/2004JD004618.

Jacobson M. 1997a. Numerical techniques to solve condensational and dissolutional growth equations when growth is coupled to reversible reactions. *Aerosol Sci. Technol.* 27: 491–498.

Jacobson M. 1997b. Development and application of a new ari pollution modelling system, Part II: aerosol module structure and design. *Atmos. Environ.* 31A: 131–144.

Jenkin M. 2004. Modelling the formation and composition of

secondary organic aerosol from α- and β-pinene ozonolysis using MCM v3. *Atmos. Chem. Phys.* 4: 1741–1757.

Jenkin M., Saunders S. & Pilling M. 1997. The tropospheric degradation of volatile organic compounds: A protocol for mechanism development. *Atmos. Environ.* 37: 81–104.

Jenkin M., Shallcross D. & Harvey J. 2000. Development and application of a possible mechamism for the generation of cis-pinic acid from the ozonolysis of α- and β-pinene. *Atmos. Environ.* 34: 2837–2850.

Jenkin M., Saunders S., Derwent R. & Pilling M. 2002. Development of a reduced speciated voc degradation for use in ozone models. *Atmos. Environ.* 36: 4725–4734.

Katoshevski D., Nenes A. & Seinfeld J. 1999. A study of processes that govern the maintenance of aerosols in the marine boundary layer. *J. Aerosol Sci.* 30: 503–531.

Korhonen H., Lehtinen K.E.J. & Kulmala M. 2004. Aerosol dynamics model UHMA: Model development and validations. *Atmos. Chem. Phys.* 4: 757–771.

Korhonen H., Kerminen V.-M. & Kulmala M. 2005. Development and application of a new analytical method to estimate the condensable vapor concentration in the atmosphere. *J. Geophys. Res.* 110, doi:10.1029/2004JD005458.

Kraabøl A., Berntsen T., Sundet J. & Stordal F. 2002. Impacts of NO_x emissions from subsonic aircraft in a global three-dimensional chemistry transport model including plume processes. *J. Geophys. Res.* 107, 4655, doi:10.1029/2001JD001019.

Kulmala M., Kerminen V.-M., Anttila T., Laaksonen A. & O'Dowd C. 2004a. Organic aerosol formation via sulphate cluster activation. *J. Geophys. Res.* 109, D04205, doi:10.1029/2003JD003961.

Kulmala M., Vehkamäki H., Petäjä T., Dal Maso M., Lauri A., Kerminen V.-M., Birmili W. & McMurry P. 2004b. Formation and growth rates of ultrafine atmospheric particles: a review of observations. *J. Aerosol Sci.* 35: 143–176.

Künzli N., Kaiser R., Medina S., Studnicka M., Chanel O., Filliger P., Herry M., Horak F., Puybonnieux-Texier V., Quénel P., Schneider J., Seethaler R., Vergnaud J.-C. & Sommer H. 2000. Public-health impact of outdoor and traffic-related air pollution: a European assessment. *Lancet* 356: 795–801.

Lohmann U. & Feichter J. 2005. Global indirect aerosol effects: A review. *Atmos. Chem. Phys.* 5: 715–737.

Lurmann F., Wexler A., Pandis S., Musarra S., Kumar N. & Seinfeld J. 1997. Modelling urban and regional aerosols-II application to California's south coast air basin. *Atmos. Environ.* 31: 2695–2715.

Nenes A., Pandis S. & Pilinis C. 1998. ISORROPIA: A new thermodynamic equilibrium model for multiphase multicomponent inorganic aerosols. *Aquat. Geoch.* 123–152.

Obot C., Morandi M., Beebe T., Hamilton R. & Holian A. 2002. Surface components of airborne particulate matter induce macrophage apoptosis through scavenger reveptors. *Toxicol. Appl. Pharmocol.* 184: 98–106.

O'Dowd C., Becker E., Mäkelä J. & Kulmala M. 2000. Aerosol physico-chemical characteristics over a boreal forest determined by volatility analysis. *Boreal Env. Res.* 5: 337–348.

O'Dowd C., Jimenez J.L., Bahreini R., Flagan R.C., Seinfeld J.H., Hämeri K., Pirjola L., Kulmala M., Jennings S.G. & Hoffmann T. 2002. Marine aerosol formation from biogenic iodine emissions. *Nature* 417: 632–636.

Pilinis C., Capaldo K., Nenes A. & Pandis S. 2000. MADM — a new multicomponent aerosol dynamics model. A*erosol Sci. Technol.* 32: 482–502.

Pirjola L., Laaksonen A., Aalto P. & Kulmala M. 1998. Sulphate aerosol formation in the Arctic boundary layer. *J. Geophys. Res.* 103: 8309–8322.

Pun B.K., Griffin R.J., Seigneur C. & Seinfeld J.H. 2002. Secondary organic aerosol 2. Thermodynamic model for gas/particle partitioning of molecular constituents. *J. Geophys. Res.* 107(D17), 4333, doi:10.1029/2001JD000542.

Raes F. 1995. Entrainment of free tropospheric aerosols as regulating mechanism for cloud condensation nuclei in remote marine boundary layer. *J. Geophys. Res.* 100: 2893–2903.

Rodriguez M. & Dabdub D. 2004. IMAGES-SCAPE2: A modeling study of size-and chemically resolved aerosol thermodynamics in a global chemical transport model. *J. Geophys. Res.* 109, D02203, doi:10.1029/2003JD003639.

Seinfeld J. & Pankow J. 2003. Organic atmospheric particulate matter. *Ann. Rev. Phys. Chem.* 54: 121–140.

Sundet J.K. 1997. *Model studies with a 3-D global CTM using ECMWF data*. Ph.D. thesis, University of Oslo.

Takemura T., Okamoto H., Maruyama Y., Numaguti A., Higurashi A. & Nakajima T. 2000. Global three dimensional simulation of aerosol optical thickness distribution of various origins. *J. Geophys. Res.* 105: 17853–17874.

Twomey S. 1977. The influence of pollution on the shortwave albedo of clouds. *J. Atmos. Sci.* 34: 1149–1152.

Vehkamäki H., Dal Maso M., Hussein T., Flanagan R., Hyvärinen A., Lauros J., Merikanto J., Mönkkönen P., Pihlatie M., Salminen K., Sogacheva L., Thum T., Ruuskanen T.M., Keronen P., Aalto P.P., Hari P., Lehtinen K.E.J., Rannik Ü. & Kulmala M. 2004. Atmospheric particle formation events at Värriö measurement station in Finnish Lapland 1998–2002. *Atmos. Chem. Phys.* 4: 2015–2023.

Wayne R. 2000. *Chemistry of atmospheres*, 3rd ed. Oxford University Press.

Wild O., Zhu X. & Prather M. 2000. Fast-j: Accurate simulation of in- and below-cloud photolysis in tropospheric chemical models. *J. Atmos. Chem.* 37: 245–282.

Zappoli S., Andracchio A., Fuzzi S., Facchini M.C., Gelencsér A., Kiss G., Krivácsy Z., Molnár Á., Mészáros E., Hansson H.-C., Rosman K. & Zebühr Y. 1999. Inorganic, organic and macromolecular components of fine aerosol in different areas of Europe in relation to their water solubility. *Atmos. Environ.* 33: 2733–2743.

Received 1 April 2005, accepted 30 June 2005